Bone regeneration around N-acetyl cysteine-loaded nanotube titanium dental implants

Young-Hee Lee[1)], Govinda Bhattarai[1)], Il-Song Park[2)], Ga-Ram Kim[2)], Go-Eun Kim[1)], Min-Ho Lee[2)], In-Ju Kim[3)], Jae-Min Seo[3)] , Seung-Geun Ahn[3)] and Ho-Keun Yi[1)]

Departments of [1)] Oral Biochemistry, [2)] Dental Biomaterials, [3)] Prosthodontics, Institute of Oral Bioscience, School of Dentistry, Chonbuk National University, Jeonju, Republic of Korea

ABSTRACT : New strategies involving drugs loading onto implant surfaces are required to enhance osseointegration and shorten healing time after implantation. In this study, we examined the feasibility of *N*-acetyl cysteine (NAC)-loaded nanotube titanium (NLN-Ti) implants as a potential drug delivery system. To determine the effect of NLN-Ti in *in vitro* and *in vivo*, viability and ROS formation was assessed and enzyme-linked immunosorbant assay (ELISA), Western blot, micro-computed tomography (μ-CT), hematoxylin and eoxin (H&E) staining and immunohistochemical (IHC) analysis were performed. *In vitro*, cell viability was increased and inflammatory responses and reduced oxidative stress-related defense were decreased with MC 3T3-E1 cells exposed to a sustained release of NAC from NLN-Ti implants. Following NLN-Ti implant installation, μ-CT and histomorphometric analysis revealed an increase of newly formed bone volume and bone mineral density in the mandibles of Sprague Dawley rats and beagle dogs. Relatively well-formed new bone was demonstrated in close contact to the NLN-Ti implant surface by H&E staining. IHC revealed a significantly higher expression of bone morphogenetic protein-2, -7 and heme oxygenase-1, and reduced the expression of the receptor activator of nuclear factor-kappa B ligand. The data indicate that NLN-Ti implants enhance osseointegration and highlight the value of the animal model in assessing diverse biological responses to dental implants.

Key Words : nanotubes, NAC, dental implant, drug delivery, osseointegration

Introduction

Enhanced osseointegration and shortened healing time are required to ensure a direct bone-to implant anchorage. However, some metabolic diseases including diabetes mellitus adversely affect the biological performance of titanium (Ti) implants, such as osteoconductive capacity[1, 2)]. Various techniques have been used to modify surface roughness, topography, chemistry and electrical charge to improve the biocompatibility and osseointegration of Ti implants because these factors are important in the biological and clinical success of implants[3, 4)]. Among the modifications to the Ti surface, the nanotube structure fabricated by anodic oxidation has demonstrated accelerated osteoblast adhesion or proliferation, and can be used as a carrier for drugs and anti-bacterial agents[5, 6)]. Furthermore, the nanotube structure is an excellent biomaterial with a high surface area-to-volume ratio and controllable dimensions for improved biocompatibility. The use of different-sized nanotubes has demonstrated an enhanced osteoblast function[7, 8)]. Although nanotubes have demonstrated benefits for bone cell-material interaction, the biological performance of nanotube structures concerning aspects like delivery of drugs, chemical compounds and bio-molecules from the implant to the bone needs to be investigated for their use in clinical applications and dental implants.

Post-implantation, the generation of inflammation and

Address of Correspondence

Ho-Keun Yi, PhD.

Department of Oral Biochemistry, Institute of Oral Bioscience, School of Dentistry, Chonbun National University, Jeonju, Republic of Korea

TEL : +82-63-270-4033 ; FAX : +82-63-270-4004 ; E-mail : yihokn@jbnu.ac.kr

its outcomes are major obstacles for implant success. It is also important to prevent the occurrence of subsequent implant failure due to a chronic inflammatory response to implant-derived wear particles or osteogenic cell stress[9, 10]. Some pathological inflammatory conditions occur from insufficiency of the cellular anti-oxidant capacity and lead to excessive production of reactive oxygen species (ROS) as well as the inflammation of the bone. ROS have been reported to be involved in bone resorption by reducing the bone mineral density[11]. Although Ti has an excellent biocompatibility, it also increases intracellular ROS levels. The harmful effects of ROS cause potential biological damage such as chronic inflammation and reduced bone regeneration[12, 13]. Hence, surface treatment of implants with antioxidants that are used as pharmacological agents is considered to reduce the inflammation via ROS scavenging, thereby enhancing bone regeneration and healing around the implant.

N-acetyl cysteine (NAC) is a cell-permeable glutathione derivative and a cysteine analogue drug with multiple therapeutic applications. NAC promotes the glutathione redox cycle as it is an amino acid derivative and an antioxidant[14]. NAC also acts as a direct ROS scavenger by increasing the cellular glutathione levels. The glutathione redox cycle is regarded as the most important regulatory mechanism for controlling oxidative stress[15]. A previous study reported that NAC-loaded pure Ti surfaces had the potential to eliminate ROS[12]. Hence, surface treatment of implants with NAC may reduce implant-induced inflammation and promote faster bone regeneration.

The conventional protocol of drug loading onto an implant surface is challenging in terms of achieving the desired cell and bone growth. Several techniques proposed for the modification of implant surfaces involve alteration of surface topography. The topography of a surface is related to the degree of biocompatibility. We previously reported that modification of the surface topography of TiO2 nanotubes with anodization increased osteoblast cell responses such as proliferation and mineralization[16]. However, the effect of drug delivery and drug release from the TiO2 nanotubes is unclear *in vitro* and after *in vivo* implantation.

In this study, we examined whether the NAC-loaded nanotube Ti (NLN-Ti) implants can be used as a potential drug delivery system and can ensure sustained release of NAC from the implant to the bone in Sprague Dawley rat mandibles after implantation.

Materials and methods

1. Preparation of materials

Commercially available pure Ti was purchased from Kobe Steel (Kobe, Japan). NAC, as the antioxidant reagent, was acquired from Sigma-Aldrich (St. Louis, MO, USA). The antibodies to SPARC (SC-25574) and HO-1 (SC-136960) were purchased from Santa Cruz Biotechnology (Santa Cruz Biotechnology, CA, USA). RANKL (AAM-425AF) was supplied by Stressgen (Ann Arbor, MI, USA). BMP-2 (BS3473) and BMP-7 (BS3674) were purchased from Bioworld (Minneapolis, MN, USA).

2. Cell culture

MC-3T3 E1 osteoblast-like cells (CRL-2593 ; American Tissue Type Collection, Manassas, VA, USA) were maintained at 37℃ in a humidified 5% CO_2 atmosphere in α-MEM (Gibco BRL, Grand Island, NY, USA) supplemented with 10% fetal bovine serum, 2 mM glutamine, 100 units/mL of penicillin and 100 μg/mL of streptomycin with sub-culture at a ratio of 1 : 4. The medium was replaced every 3 days and cells were used at 80% confluence.

3. Preparation of pure Ti, TiO2 and NAC loading

Commercially pure titanium foil (99.9% purity, Kobe Co., Japan) in each size was polished incrementally with 400-grit to 1,000-grit emery paper, and then washed with acetone and distilled water in an ultrasonic cleaner. TiO2 nanotubes were fabricated using an anodization process as described previously[16]. Anodic oxidation was performed under potentiostatic control, and the measurements were made in an electrolyte solution consisting of NH_4F : H_2O : glycerol at a ratio of 1 : 20 : 79 wt.% in a glass chamber using a direct-current power-supply system (SP6303, Samwoo Elect., Korea). The voltage and current density were 20 V and 30 mA/cm^2 respectively, applied for 1 h at room temperature. The nanotube structure on Ti was analyzed by Field Emission Scanning Electron Microscopy (FE-SEM) using a SUPRA40VP apparatus (Carl Zeiss, Jena, Germany). Pure and nanotubes Ti were used at dimensions of 1 x 1 cm x 1 mm and 6 x 6 cm x 1 mm *in vitro* and, pure and nanotube Ti mini screws with a length of 4.5 mm and a diameter of 0.85 mm were used for *in vivo* dental implants. The preparations were cleaned with deionized water prior to loading of the NAC solution. Briefly, 10 mM of NAC solution was prepared in autoclaved distilled water. Each Ti surface was immersed in the NAC

solution and incubated for 24 h and allowed to dry under vacuum at room temperature for 24 h. After drying, the loading step was repeated until the appropriate amount of NAC was evenly coated on each Ti surfaces. Following terms were used to specify the each implant-to pure Ti : P-Ti, NAC-loaded pure Ti : NLP-Ti, nanotube Ti : N-Ti and NAC-loaded nanotube Ti : NLN-Ti in this experiment

4. Measurement of the contact angle

For the assessment of surface hydrophobicity and hydrophilicity, surface wettability was measured by dropping 10 μl distilled water onto the surface at a location 5 cm away from the surface. The shape of the water drop that was formed was photographed using a DE/EZ 4 stereoscopic microscope (Leica Microsystems, Wetzlar, Germany) and the contact angle was measured using the National Institutes of Health Image J software.

5. Testing of NAC release from Ti surfaces using an indirect method

The amount of NAC released from the pure and nanotube Ti surfaces (fiat ; 1 x 1 cm x 1 mm) was detected using a V-630 UV-VIS spectrophotometer (Jasco, Easton, USA). From the day of NAC loading, each specimen was immersed in 1 mL of autoclaved distilled water in a 24-well plate at room temperature with shaking at 50 rpm. Samples were transferred to microcentrifuge tubes every other day and stored at 4℃. The amount of drug release was measured by a UV detector at 290 nm[17]. A standard curve for the known concentration of NAC was used to determine the unknown concentration.

6. Cell viability assays

The 3-(4, 5-dimethylthiazol-2-yl)-2, 5-diphenyltetrazolium bromide (MTT) assay was used to determine the cell viability. MC-3T3-E1 cells were seeded on the pure Ti, nanotube Ti (1 x 1 cm x 1 mm) and Ti surfaces loaded with designated amounts of NAC, placed into 24-well tissue culture plates at a density of 2 x 10^5 cells and incubated for 48 h. At the end of the incubation period, the samples were rinsed twice with sterile phosphate buffered saline (PBS) and the adherent cells were incubated in medium containing 100 μg/0.1 mL of MTT (Sigma-Aldrich) for 4 h. After carefully removing the medium, the purple formazan product was dissolved in dimethyl sulfoxide and the optical density (OD) values were recorded using a Synergy 2 spectrophotometer (Bio-Tek Instruments, Winooski, VT, USA) at 570 nm to determine the cell viability.

For crystal violet staining, the cells on titanium were fixed with 2% paraformaldehyde, 0.2% glutaraldehyde in PBS for 15 min at room temperature. After washing with PBS, cells were incubated with 0.3% crystal violet solution for 30 min at room temperature. The cells were washed twice with PBS and visualized using a model BX60MF stereo microscope (Olympus, Tokyo, Japan).

7. Total nitric oxide (NO) analysis

The NO concentrations in the medium were measured using the total NO assay kit (Assay Designs/Stressgen) by the modified Griess reaction[18]. The calculated concentration was taken as an indicator of NO production. MC-3T3-E1 cells were seeded on the pure Ti, nanotube Ti (1 x 1 cm x 1 mm) and Ti surfaces loaded with amount of NAC and placed into 24-well tissue culture plates at a density of 2 x 10^5 cells and incubated for 48 h. One hundred microliters of each supernatant was mixed with assay buffer according to the manufacturer's instructions. The absorbance was measured at 550 nm using a Synergy 2 ELISA plate reader (Bio-Tek Instruments).

8. Cytokine measurement

Cytokine concentration in the supernatants was determined by ELISA. MC-3T3-E1 cells were seeded on the pure Ti, nanotube Ti (1 x 1 cm x 1 mm) and Ti surfaces loaded with amount of NAC and placed into 24-well tissue culture plates at a density of 2 x 10^5 cells and incubated for 48 h. The levels of tumor necrosis factor-alpha (TNF-α) and interleukin (IL)-1β were analyzed using an OptEIA ELISA kit (BD Biosciences, San Jose, CA, USA) according to the manufacturer's instructions. One hundred microliters of each supernatant was mixed with assay buffer according to the manufacturer's instructions. The absorbance was measured at 420 nm as described above.

9. Measurement of ROS formation

Generation of ROS was assessed by using the oxidation sensitive fluorescent probe 2',7'-dichlorodihydrofluore scein diacetate (DCFH-DA ; Sigma-Aldrich). The cells were detached from Ti surfaces and incubated with 5 μM DCFH-DA for 30 min at 37 ℃. ROS formation was analyzed by FACScan flow cytometry (Becton-Dickinson, Franklin Lakes, NJ, USA).

10. Western blot analysis

Total protein was extracted from the MC-3T3-E1 cells using a lysis buffer containing 150 mM NaCl, 5 mM EDTA,

50 mM Tri-HCl (pH 8.0), 1%-NP 40, 1 mM aprotinin, 0.1 mM leupeptin and 1 mM pepstatin and quantified using the Bradford dye-binding procedure (Bio-Rad, Hercules, CA, USA). A total of 20 μg protein was subjected to 8% sodium dodecyl sulfate-polyacrylamide gel electrophoresis under denaturing conditions and the resolved proteins were transferred to a Hybond-P membrane (Amersham, Arlington, IL, USA) using the Mini-protean II system (Bio-Rad). After blocking with 5% skimmed milk in PBS, the membranes were incubated with the appropriate antibody at a 1 : 1,000 dilution in either 1% skim milk or 3% bovine serum albumin for 4 h or 24 h at 4 ℃ or room temperature. After washing with PBS containing 0.1% Tween-20, once for 15 min and twice for 5 min, the membranes were incubated with anti-mouse or anti-rabbit IgG antibody conjugated to horseradish peroxidase at a 1 : 3,000 dilution in PBS for 1 h at room temperature. The signals were visualized by chemiluminescent detection according to the manufacturer's protocol (Amersham Pharmacia Biotech, London, UK) and detected by LAS-4000 scanner (Fuji Film, Tokyo, Japan). The protein expression levels were analyzed with ImageQuanT TL 1D gel analysis program (GE Healthcare, Bio-Science, Sweden).

11. Animals and surgical procedures

For *in vivo* experiments, 20 eight-week-old male Sprague Dawley rats were obtained from Damule Science Animal Laboratory (Daejeon, Korea). The study protocol was approved by the Ethical Committee of Chonbuk National University. All surgical procedures were performed under general anesthesia induced with Zolazepam (Zoletil 50 ; Virbac Carros, France) and xylazine hydrochloride (Rompun ; Bayer Korea, Seoul, Korea) under veterinary supervision. The lower first molar was extracted carefully to avoid damage to the extraction socket. After determining that the alveolar bone had healed well one month after the extraction, implant placement was performed. All Ti specimens were used : pure Ti specimens (P-Ti) (n=5), nanotube Ti specimens (N-Ti) (n=5), pure Ti specimens loaded with NAC (NLP-Ti) (n=5) and nanotube Ti specimens loaded with NAC (NLN-Ti) (n=5). The implant site was prepared using a 0.8 mm diameter drill. The implants were inserted after making a hole with a drill at a low speed (900 rpm) with saline irrigation to avoid heating. Implantation was considered successful when, at the end of the experimental period, the implant showed no signs of mobility in situ. All rats were reared in individual cages where in the temperature was maintained at 20 to 25℃ and the relative humidity at 30 to 50%. Post-operative antibiotic treatment, according to the body weight, was administered by injection into the rats twice daily for four days.

Also, four beagle dogs of twelve months old (weighing approximately 15.5kg) were used for histomorphometric analysis. Both mandibular premolars and 1st molar were extracted. 20 weeks after the extraction, each experimental implant fixtures were placed. Two beagle dogs were sacrificed after 3 weeks and the other two dogs were sacrificed after 6 weeks from implant installation.

12. Micro computed tomography (μ-CT) analysis

μ-CT was performed using a model 1076 apparatus (Skyscan, Kontich, Belgium) operating with an anode electrical current of 100 kV with an aluminum filter for elimination of the hardening beam at a resolution of 18 μm. After implantation, the rats in each group were anesthetized and the mandibles were scanned by μ-CT to evaluate the dynamic changes in the peri-implant tissue at 1, 2 and 4 weeks. The regions of interest (ROI) that included the mandible compartment around implants were selected. After scanning, three-dimensional (3D) models were generated by CTVol (Skyscan), and bone volume and density around implants were analyzed by the CTAn program (Skyscan), which was also used to examine the μ-CT data sets for new bone growth. The volume of interest (VOI) consisted of the collective sum of all ROI layers over continuous set of cross-sectional image slices. This represents the regenerated bone only. Further, new bone volume and bone mineral density around the implant was calculated by the phantom and Housefield units [HU]. A bone and implant threshold value in CT HU was determined between low phantom (0.25) 1089.7966 HU and high phantom (0.75) 3241.0643 HU. Based on this threshold, a distinction between bone and no bone volume elements can be made. As the volume of ROI corresponds to the volume of original bone, the amount of bone present within the ROI is considered as the new formed bone. To create 3D images binary threshold (Gray scale index, implant area ; 160～255 μm, new bone area ; 100～143 μm and total bone area ; 70～120 μm) were selected.

13. Histology (H&E) staining and immunohistochemical (IHC) staining

The mandible with the implants were isolated and fixed in 10% neutral-buffered formalin solution. After

decalcification in 15% EDTA and 0.1 M Tris (pH 7.0), the implants were gently removed, and the mandibular tissues were dehydrated, cleared and embedded in paraffin. Tissue sections, 8 μm in thickness, were mounted on glass slides and subjected to IHC and H&E staining. IHC staining was performed to detect the expression of bone morphogenetic protein (BMP)-2, -7, RANKL and heme oxygenase (HO)-1 using the Immunohistochemistry accessory kit (Bethyl Laboratories Montgomery, TX, USA). The each primary antibody was used at a 1 : 200 dilution following the protocol. The slides were observed by microscopy (Carl Zeiss, Ostalbkreis, Germany) and cell counts were performed in the newly formed bone area, which was restricted to the 0.5 mm area surrounding the implants.

14. Histomorphometric analysis

The stained histologic specimens were scanned and captured using optical microscopy at 12.5x, 40x and 100x magnification. The ratio for bone-to-implant contact (BIC %) was calculated except apical cutting edge of the implant.

15. Statistical analysis

All results of the control and experimental groups were analyzed independently. We used one-way ANOVA at a significance level of $p < 0.05$ to examine the differences in the variables among different experimental conditions.

Results

1. Characterization of NLN-Ti surface and NAC release test

The nanotube structure was fabricated on Ti by anodic oxidation using voltage of 20 V for 1 h. The morphology of nanotube structure was dense and the nanotubes were approximately 50 ± 15 nm in diameter and 1.26 μm by FE-SEM analysis (Fig. 1A). This depicts that typical nano tube structure was formed by anodization method. Surface contact angle was measured for assessing the hydrophobicity and hydrophilicity of the different surfaces (pure Ti : P-Ti, NAC-loaded pure Ti : NLP-Ti, nanotube Ti: N-Ti and NAC-loaded nanotube Ti : NLN-Ti). The contact angle of water on the P-Ti surface was 50.5°, which indicated hydrophobicity of the surface, while both the NLP-Ti and NLN-Ti with N-Ti surfaces demonstrated a hydrophilic behavior. However, NLN-Ti displayed much more optimized hydrophilic behavior (Fig. 1B).

To perform NAC loading on both the pure and nanotube Ti surfaces, the Ti surfaces were immersed in the 10 mM NAC solution. Fig. 1C shows the results of NAC release for 7 days by UV-VIS spectrophotometry after performing the immersion step. The NAC as a kwon concentration was detected at 290 nm in the reference (Fig. 1C, left). On day 1, the amount of NAC was released more from and N-Ti surfaces than the P-Ti surfaces (approximately 0.3 mM). Two days after the release tests, the P-Ti surface demonstrated a remarkable decrease in the amount of NAC released from the surface (<0.1 mM), while the N-Ti surface demonstrated a continuously higher amount of NAC release and sustained release until day 4 (Fig. 1C). These findings indicate that NAC is avidly loaded onto the nanotubes and is able to sustain release from the nanotubes to the bone area for a longer time.

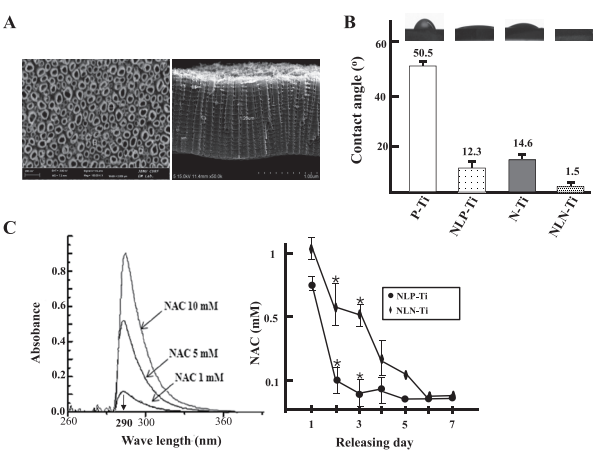

Fig. 1 Field emission scanning electron microscopy analysis of fabricated nanotube structures frontal view (left panel) and lateral view (right panel) (A), average contact angles (P-Ti ; pure-Ti, NLP-Ti ; NAC-loaded pure-Ti, N-Ti ; nanotube-Ti and NLN-Ti ; NAC-loaded nanotube-Ti) (B), release of NAC at 7 days by UV spectrum (C).

2. NLN-Ti surface enhances cell viability and osteogenic molecules via reduction of the inflammatory response in MC-3T3 E1 cells in vitro

To investigate the effect of NAC loading on MC-3T3 E1 cells seeded on the pure and nanotube Ti surfaces, the cell viability was assessed by the MTT assay and crystal violet staining assay. The NLN-Ti surface displayed increased cell viability compared to the NLP-Ti surface at 48 h. The NLP-Ti surface showed increased cell viability than the N-Ti surface. Furthermore, it was observed that the NLN-Ti surface prevented ROS formation similar to that in normal cells (Fig. 2C). However, there was no significant difference in cell growth between the P-Ti surface and the N-Ti surface (Fig. 2A, B).

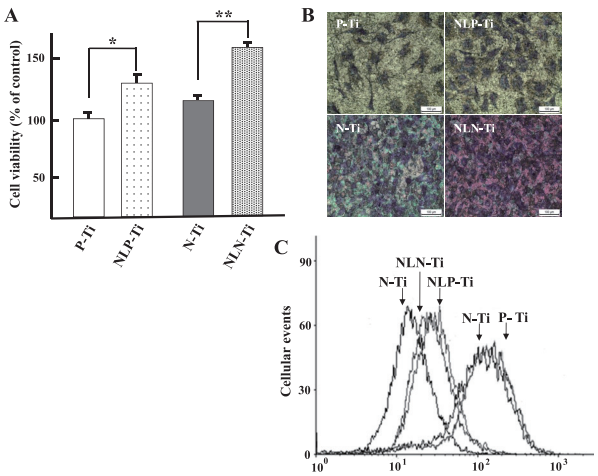

Fig. 2 Cell viability, morphology and ROS formation in MC-3T3-E1 cells seeded on the implant surfaces.

Cells (1 x 10^5) were seeded on P-Ti and N-Ti surfaces without or with NAC loading. The cell viability was determined using a MTT assay at 48 h (A) and the morphology of the cultured cells was determined using a crystal violet staining assay by stereo microscopy at 48 h (B), the level of ROS production on cells seeded on titanium surfaces was determined by flow cytometry after the DCFH-DA treatment at 48 h and was compared with that on cells seeded on non Ti surfaces (C). Each value is reported as the mean and standard error of the mean (S.E.M) of three independent experiments.

*$p < 0.05$ indicate significance

The NAC reduction in the inflammatory response was evaluated based on the secretion of inflammatory cytokines. The up-regulation of NO production and cytokines such as TNF-α and IL-1β in cells are one of the critical indicators of inflammatory responses. An almost basal level of NO was detected in MC-3T3-E1 cells seeded on untreated Ti surfaces, while the level of NO production in MC-3T3-E1 cells after lipopolysaccharide (LPS)-induced inflammatory responses was 139 ± 0.5 μmol/L in the culture supernatants from both the pure and nanotube Ti surfaces. In this study, LPS was used for inducing inflammatory responses. However, the production of NO in cells seeded on both the NLP-Ti and NLN-Ti surfaces was significantly inhibited even under LPS stimulation at 48 h (Fig. 3A). Also, the production of pro-inflammatory cytokines such as TNF-α and IL-1β was significantly inhibited in the cells seeded on both the NLP-Ti and NLN-Ti surfaces at 48 h (Fig. 3B, 3C). However, the NLN-Ti surface exhibited a tendency for good cell growth and reduction in inflammation for new bone formation compared to the NLP-Ti surface (Fig. 2A, B, 3A-C) at 48 h.

The development of osteogenic molecules in cells after NAC loading on both the pure and nanotube Ti surfaces

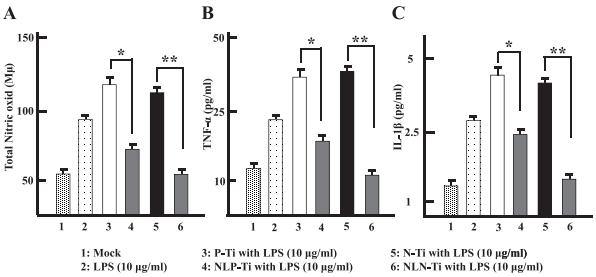

Fig. 3 Expression of pro-inflammatory cytokines was reduced in MC-3T3 E1 cells seeded on NAC-loaded Ti surfaces.

Cells (1 x 10^5) seeded on P-Ti and N-Ti surfaces with NAC loading or without NAC were stimulated with LPS. After 48 h of incubation, the levels of NO (A), pro-inflammatory cytokines TNF-α (B) and IL-1β (C) were measured in the culture supernatant using ELISA. Data represent the mean value of triplicate determinations.

*$p < 0.05$ indicates significance

was assessed by immunoblotting at 48 h. High expression levels of osteogenic molecules (BMP-2 and BMP-7) and cell adhesion molecules (SPARC) were evident in MC-3T3-E1 cells after NAC loading on both the pure and nanotube Ti surfaces. Interestingly, the cells grown on NLN-Ti surface demonstrated a significant inhibition of osteogenic inflammatory molecules (RANKL) (Fig. 4A).

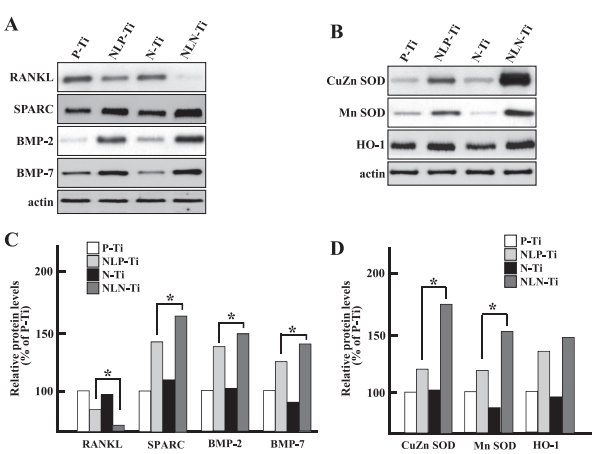

Fig. 4 MC-3T3 E1 cells seeded on NAC-loaded Ti surfaces show anti-inflammation and increased expression of osteogenic molecules.

Cells (5 x 10^5) were seeded on P-Ti and N-Ti with NAC loading or without NAC. The expression of RANKL, SPARC, BMP-2 and -7 proteins in the total cell lysate was determined by Western blot analysis at 48 h (A), and levels of oxidative stress defense markers Cu/Zn SOD, Mn SOD and HO-1 protein level were determined by Western blot (B). For loading control, the blots were reprobed with actin antibody. The expression of the immunoreactive bands was measured by the ImageQuant TL 1D gel analysis program. Densitometry results in percentage are shown as a bar graph. Data are expressed as mean ± SEM (n=3).

*$p < 0.05$ by one way Anova plus Scheffe test.

In addition, NAC loading on both pure and nanotube Ti augmented the level of defense molecules against oxidative stress such as Cu/Zn superoxide dismutase (SOD), Mn SOD and HO-1 in MC-3T3-E1 cells (Fig. 4B). The molecular density of proteins was different in each group (Fig. 4C, D).

3. Effect of bone formation on NLN-Ti in vivo by μ-CT analysis in rat mandible

We examined whether the nanotube surface and pharmacological activity of NAC influenced bone formation in rat mandible after implantation. For *in vivo* implantation in Sprague Dawley rats, the lower first molar was extracted and a one month period was allowed for complete healing. μ-CT analysis was carried out for structural and quantitative assessments of new bone formation and mineralization post-implantation in the defective site. We conducted μ-CT analysis to identify a suitable implant site and to assess newly bone restored. Two-dimensional (2D) μ-CT images showed the morphology of tooth before extraction and after extraction, and the restoration by new bone at the extraction site on different days. At 4 weeks, the extraction site was completely healed (Fig. 5A). After 4 weeks, P-Ti, NLP-Ti, N-Ti and NLN-Ti implants were inserted into the healing site of the mandible. After implantation, the images clearly demonstrated suitable implantation sites and new bone formation around the implant site in a time-dependent manner. At the first week post-implantation, the new bone formation on implant surface was not significantly different between the pure Ti surface and the nanotube Ti surface, even with NAC loading. However, at 4 weeks post-implantation, 2D images revealed the successful anchorage of NLN-Ti implants, but not NLP-Ti implants (Fig. 5B). Typically, new bone formation and bone mineral density around the NLP-Ti and NLN-Ti implants was evaluated by three dimensional (3D) image analyses. The 3D images clearly demonstrated more new bone formation on the NLN-Ti surface (Fig. 5C ; panels e-h) than on the NLP-Ti surface (Fig. 5C ; panels a-d). Furthermore, the volume of the newly formed bone and bone mineral density were significantly enhanced around the NLN-Ti surface than around the NLP-Ti surface at 4 weeks post-implantation (Figs 5D, E). However, there was no significant difference in the bone volume and mineral density between P-Ti implants and the N-Ti implants (data not shown).

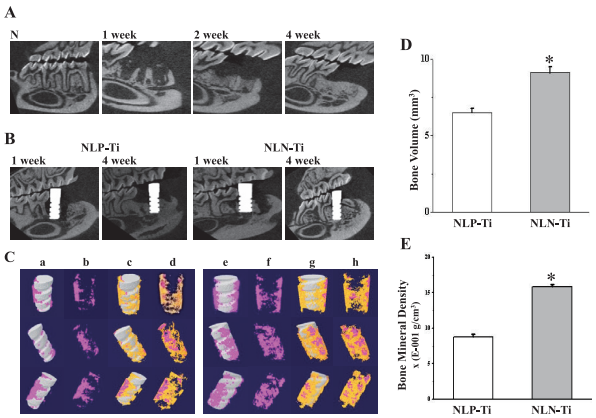

Fig. 5 μ-CT analysis indicates that implants are successfully inserted in the correct position and new bone formation occurs.
In the in vivo model, lower first molars of Sprague-Dawley rats were extracted and the extraction site was allowed to heal for duration of 1, 2 and 4 weeks (A), and the changes in the peri-implant tissue and position of NLP-Ti and NLN-Ti implants were determined at 1 week and 4 week by 2D μ-CT monitoring (B). After 4 weeks, the thickness of the newly formed bone surrounding the implant was determined by 3D μ-CT ; gray represents the implant and pink and yellow represents the bone tissue (C), and 3D analysis of the volume of the newly formed bone (D), and bone mineral density (E) around the NLP-Ti and NLN-Ti implants. Data are expressed as mean ± SEM at 4 weeks (n=5).
*$p < 0.05$

4. Effect of NLN-Ti on bone regeneration in rat mandible by histological assessments

At 4 weeks post-implantation, new bone formation around both NLP Ti and NLN Pi implants was assessed by H&E staining. The newly formed bone around the NLP-Ti implant was immature bone and there was little growing of bone in implant around (Fig. 6A). In addition, loosely organized, inflammatory infiltrate and irregular bone trabeculae with a few osteoblasts were observed on NLP-Ti implants (Fig. 6B). In contrast, a relatively well formed new bone with regular bone trabeculae was observed at implant sites around the NLN-Ti (Fig. 6C, D). Moreover, the bone was consistency uniform and in close contact with the implant surface with good lamination and abundant osteocytes (Fig. 6D, arrow). However, poor bone formation and more inflammatory infiltrate were observed around the P-Ti and the N-Ti implants on the same days (data not shown).

At 4 weeks post-implantation, IHC staining was performed to evaluate osteogenic differentiation and reduction of inflammatory effect of NAC loading on both pure and nanotube Ti implants. The expression of

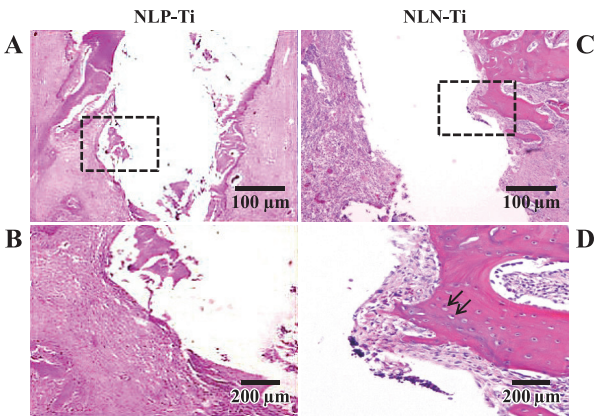

Fig. 6 Histomorphological analysis by hematoxylin & eosin staining.

At 4 weeks post-implantation, the photomicrographs showed different histological morphologies from H&E staining. NLP-Ti implant surfaces showed immature bone formation and little bone-implant contact (A and B), and the NLN-Ti implant surfaces showed a well formed new bone and regular bone trabeculae with lamination and abundant osteocytes (C and D). At least five slides of each specimen were observed.

BMP-2 (Fig. 7A, B) and -7 (Fig. 7C, D), as the markers for osteogenic differentiation, was more intense around NLN-Ti implants than around NLP-Ti implants. Also, the expression of the bone inflammatory marker RANKL was clearly less intense in the newly formed bone area around NLN-Ti implants than around NLP-Ti implants (Fig. 8A, B). Furthermore, more intense expression of the HO-1 anti-oxidant molecules was observed around NLN-Ti implants than around NLP-Ti implants (Fig. 8C, D).

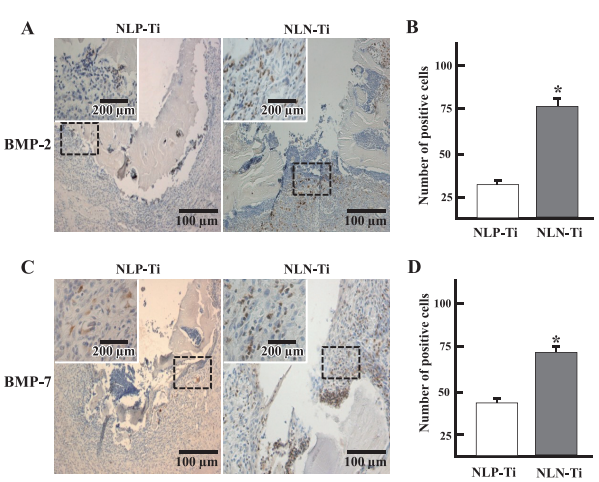

Fig. 7 Effect of NAC loading onto surfaces of Ti nanotube implants on the expression of BMP-2 and -7.

At 4 weeks after implantation, the expressions of BMP-2 (A, B), and -7(C, D) were analyzed by immunohistochemistry. Data are expressed as mean ± SEM (*$p < 0.05$). The brown color indicates positive cells.

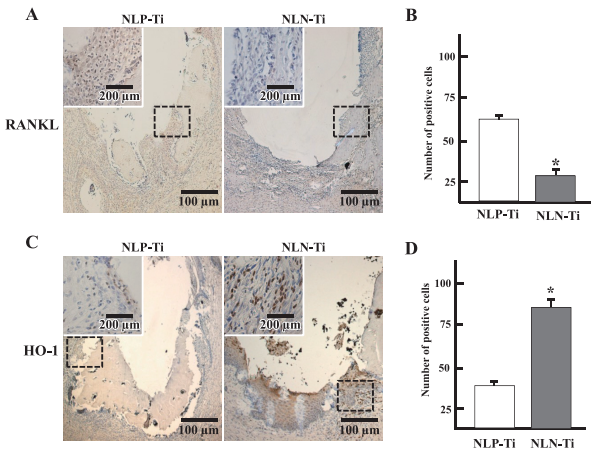

Fig. 8 Effect of NAC loading onto surfaces of Ti nanotube implants on the expression of RANKL and HO-1.

At 4 weeks after implantation, the expressions of RANKL (A, B), and HO-1 (C, D) were analyzed by immunohistochemistry. Data are expressed as mean ± SEM (*$p < 0.05$). The brown color indicates positive cells.

5. Histomorphometric findings

In both groups of 3 and 6 weeks, the NNI showed higher BIC ratio than the non-treated group (Fig. 9).

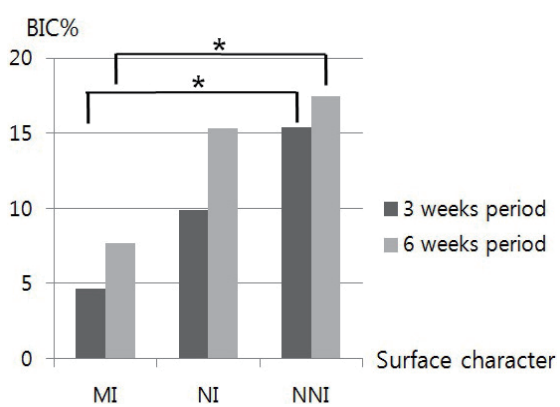

Fig. 9 Bone to implant contact percentage (BIC%) of machined implant (MI), TiO_2 nanotube implant (NI), NAC-loaded TiO_2 nanotube implant (NNI).

*A significant difference was determined ($P<0.05$).

Discussion

New strategies in which drugs loaded onto the surface of implants surface are delivered to the bone tissue may enhance osseointegration and shorten the healing time after implantation. Ti and its alloys have exhibited favorable bioactivity via modification of the implant surface. Current techniques suggest drug loading into nanotubes on the implant surfaces as a means of surface modification[6]. The biological effect of NAC on Ti surfaces has been reported to improve osseointegration

and osteoconductive capacity[12, 19, 20]. However, there is insufficient data in the literature concerning the biological mechanisms in vitro and *in vivo* for a successful clinical outcome after implantation.

In this study, NAC was loaded on nanotube Ti implants with the aim of enhancing bone regeneration and osseointegration through the sustained release of NAC. The Ti nanotube structure (pore size of approximately 50 ± 15 nm, length of 1.26 μm) was obtained by a simple anodization technique using an anodization voltage of 20 V and a current of 30 mA/cm^2 for 1 h. NAC-loaded Ti surfaces displayed small contact angles compared to those of non-loaded Ti surfaces. Interestingly, NLN-Ti surfaces had significantly smaller contact angles than those of NLP-Ti surfaces. In addition, NLN-Ti surfaces exhibited sustained release of NAC for 5 days. Ti nanotubes have proven to be a suitable vehicle for the loading and sustained elution of drugs, chemicals and biomolecules [6, 21]. We previously reported that fabricated nanotubes have a hydrophilic surface that promotes ready attachment of cells[16, 21]. These results indicate that the Ti nanotube structure increases the wettability surface energy via the quantity of interpenetrating NAC and allow easy organic modification of the implant surface. Also, the sustained release of NAC may be pivotal in enhancing cell attachment and osseointegration.

The condition of implant surfaces leads to exacerbated inflammatory responses and impaired response of bone and periodontal tissues following implant placement[12, 22, 23]. The use of dental implants in pathological conditions including metabolic diseases is required in therapeutic strategies due to the adverse effects on osseointegration[1, 2]. Overproduction of ROS and nitric oxide (NO) causes cellular dysfunction in osteoblasts and is involved in the pathogenesis of diseases including rheumatoid arthritis and autoimmune diabetes[24]. Among the pro-inflammatory cytokines, TNF-α and IL-1β are the primary mediators of inflammatory responses. They are associated with various chronic inflammatory diseases[25, 26]. In this study, under LPS-induced inflammatory conditions, increased NO production and higher secretion of TNF-α and IL-1β were observed in MC-3T3-E1 osteoblast-like cells. Increased secretion of pro-inflammatory cytokines and excessive ROS formation on implant surfaces was also evident. However, both Ti implant surfaces loaded with NAC showed diminished secretion of these cytokines and ROS formation. NAC-loaded implants enhanced cell viability as compared to implant surfaces devoid of NAC. Subsequently, MC-3T3-E1 cells seeded on pure Ti and nanotube Ti surfaces increased the expression of RANKL and markedly diminished the expressions of BMP-2, -7 and SPARC. In addition, defense molecules against oxidative stress, such as Cu/Zn SOD, Mn SOD and HO-1, were down-regulated in cells seeded on these Ti surfaces. However, opposite findings were observed with cells seeded on the NLP-Ti and NLN-Ti surfaces. Compared with NLP-Ti, NLN-Ti surfaces attenuated the level of RANKL expression and expression of oxidative stress defenses molecules, such as Cu/Zn SOD, Mn SOD and HO-1, and bone formation molecules, such as BMP-2 and -7. Oxidative stress leads to an inflammatory response, osteoclast differentiation and bone destruction via activation of RANKL and osteoblast dysfunction[19, 26]. RANKL is the key molecule that regulates bone destruction. Its expression stimulates osteoclastogenesis, which lead to bone resorption[27, 28]. SPARC is an extracellular matrix protein that modulates mineralization[29]. In addition, the inflammatory response influences the expression of osteogenic molecules including BMP-2 and -7[26]. NAC promotes an increase in osteoblasts and reducing of inflammatory molecules[12, 19, 20]. The collective data strongly suggests that the surface of Ti nanotubes is suitable for drug loading on dental implants, and that NAC promotes osteoblastic function via its antioxidant effects, thereby improving the degree of osseointegration.

We attempted to develop a Sprague-Dawley rat mandibular model to probe the effect of NAC loading on the surfaces of Ti nanotube implants *in vivo*. Implants were inserted following the extraction of the right lower first molars of rats, and we waited for one month for achieve complete healing. This is a simple animal model for assessing the biological response after implantation. μCT imaging was useful in measuring the temporal process of tissue-implant integration *in vivo* and was beneficial for determining the accurate amount of bone formation around the implant surfaces. 3D μCT allowed detection of mineralized tissue and new bone formation[30, 31]. Hence, we used mini screw Ti constructs as a relevant model for dental implants and μCT monitoring for evaluating adequacy of implant insertion and new bone formation on the implant surfaces in the *in vivo* model. After tooth extraction, complete healing of the extraction sites was demonstrated at 4 weeks by μCT monitoring. This time period of healing is typical, since the maxillary bone typically heals within one month, thereby allowing installation of oral implants[32]. Owing to the empty spaces,

the main concerns of this study were to achieve loading of NAC onto the nanotubes and their delivery to the bone tissue.

We desired to evaluate the effects of NAC loading on nanotube surfaces and delivery of NAC as a vital drug to increase osseointegration around the dental implants. At 1 and 4 weeks post-implantation, 2D μCT images showed that the implant was inserted in the correct position. There was new bone formation around the NLN-Ti implants at 4 weeks. Furthermore, 3D μCT analysis revealed new bone formation and increased bone mineral density around the NLN-Ti implants at 4 weeks. Moreover, using H&E staining the NLN-Ti implant surfaces showed regular bone trabeculae with abundant osteocytes at 4 weeks. However, the NLP-Ti surfaces showed poor histopathological findings, such as irregular bone trabeculae and fewer ostetocytes, under the same conditions. IHC revealed augmented the expression of osteogenic molecules including BMP-2 and -7, and attenuated expression of RANKL around the NLN-Ti implant. Especially noteworthy was the *in vivo* expression of the HO-1 anti-oxidant following installation of NAC surface-loaded implants. Thus, the loading of NAC on surfaces of Ti nanotube implants may increase osteogenesis, and promote bone regeneration and osseointegration, enhancing bone-remodeling and implant stability. The Ti nanotube implants facilitated drug delivery and caused an increase in the volume of the newly formed bone and bone mineral density around the dental implants.

Several studies have assessed the hard tissue response at the bone-implant interface as a biomechanical property of dental implants[30, 31, 32]. However, these studies provided limited information regarding the biological response *in vivo*. Altering the surface topography of dental implants leads to early bone regeneration[4, 33]. This study provides evidence regarding the effect of NLN-Ti implant for achieving a higher degree of osseointegration in hard tissue such as mandibules for dental implant.

Conclusion

This study provides information regarding the applicability of nanotubes in delivery of drugs, chemicals and bio-molecules including NAC for a successful dental implantation. Also, the animal study was useful for assessing diverse biological responses to dental implants.

References

1) Javed F, Romanos GE : Impact of diabetes mellitus and glycemic control on the osseointegration of dental implants : a systematic literature review. J Periodontol 80 : 1719-1730, 2009.
2) Prisby RD, Swift JM, Bloomfield SA, Hogan HA, Delp MD : Altered bone mass, geometry and mechanical properties during the development and progression of type 2 diabetes in the Zucker diabetic fatty rat. J Endocrinol 199 : 379-388, 2008.
3) Förster Y, Rentsch C, Schneiders W, Bernhardt R, Simon JC, Worch H, et al : Surface modification of implants in long bone. Biomatter 2 : 149-157, 2012.
4) Kim TI, Jang JH, Kim HW, Knowles JC, Ku Y : Biomimetic approach to dental implants. Curr Pharm Des 14 : 2201-2211, 2008.
5) Brammer KS, Oh S, Cobb CJ, Bjursten LM, van der Heyde H, Jin S : Improved bone-forming functionality on diameter-controlled TiO(2) nanotube surface. Acta Biomater 5 : 3215-3223, 2009.
6) Popat KC, Eltgroth M, Latempa TJ, Grimes CA, Desai TA : Decreased Staphylococcus epidermis adhesion and increased osteoblast functionality on antibiotic-loaded titania nanotubes. Biomaterials 28 : 4880-4888, 2007.
7) Balasundaram G, Yao C, Webster TJ : TiO2 nanotubes functionalized with regions of bone morphogenetic protein-2 increases osteoblast adhesion. J Biomed Mater Res A 84 : 447-453, 2008.
8) Das K, Bose S, Bandyopadhyay A : TiO2 nanotubes on Ti : influence of nanoscale morphology on bone cell-materials interaction. J Biomed Mater Res A 90 : 225-237, 2009.
9) Holt G, Murnaghan C, Reilly J, Meek RM : The biology of aseptic osteolysis. Clin Orthop Relat Res 460 : 240-252, 2007.
10) Mavrogenis AF, Dimitriou R, Parvizi J, Babis GC : Biology of implant osseointegration. J Musculoskeletal Neuronal Interact ; 9 : 61-71, 2009.
11) Basu S, Michaëlsson K, Olofsson H, Johansson S, Melhus H : Association between oxidative stress and bone mineral density. Biochem Biophys Res Commun 19(288) : 275-279, 2001.
12) Lee YH, Lee NH, Bhattarai G, Oh YT, Yu MK, Yoo ID, et al : Enhancement of osteoblast biocompatibility on titanium surface with terrein treatment. Cell Biochem Funct 28 : 678-685, 2010.

13) Eckhardt A, Gerstmayr N, Hiller KA, Bolay C, Waha C, Spagnuolo G, et al : TEGDMA-induced oxidative DNA damage and activation of ATM and MAP kinases. Biomaterials 30 : 2006-2014, 2009.
14) Zafarullah M, Li WQ, Sylvester J, Ahmad M : Molecular mechanisms of N-acetylcysteine actions. Cell Mol Life Sci 60 : 6-20, 2003.
15) Meister A, Anderson ME. Glutathione : Annu Rev Biochem 52 : 711-760, 1983.
16) Park IS, Lee MH, Bae TS, Seol KW : Effects of anodic oxidation parameters on a modified titanium surface. J Biomed Mater Res B Appl Biomater 84 : 422-429, 2008.
17) Wu W, Goldstein G, Adams C, Matthews RH, Ercal N : Separation and quantification of N-acetyl-l-cysteine and N-acetyl-cysteine-amide by HPLC with fluorescence detection. Biomed Chromatogr 20 : 415-422, 2006.
18) Dirsch VM, Stuppner H, Vollmar AM : The Griess assay : suitable for a bioguided fractionation of anti-inflammatory plant extracts? Planta Med 64 : 423-426, 1998.
19) Feng YF, Wang L, Zhang Y, Li X, Ma ZS, Zou JW, et al : Effect of reactive oxygen species overproduction on osteogenesis of porous titanium implant in the present of diabetes mellitus. Biomaterials 34 : 2234-2243, 2013.
20) Yamada M, Minamikawa H, Ueno T, Sakurai K, Ogawa T : N-acetyl cysteine improves affinity of beta-tricalcium phosphate granules for cultured osteoblast-like cells. J Biomater Appl 27 : 27-36, 2012.
21) Moon SH, Lee SJ, Park IS, Lee MH, Soh YJ, Bae TS, et al : Bioactivity of Ti-6Al-4V alloy implants treated with ibandronate after the formation of the nanotube TiO2 layer. J Biomed Mater Res B Appl Biomater 100 : 2053-2059, 2012.
22) Tsaryk R, Kalbacova M, Hempel U, Scharnweber D, Unger RE, Dieter P, et al : Response of human endothelial cells to oxidative stress on Ti6Al4V alloy. Biomaterials 28 : 806-813, 2007.
23) Aziz-Kerrzo M, Conroy KG, Fenelon AM, Farrell ST, Breslin CB : Electrochemical studies on the stability and corrosion resistance of titanium-based implant materials. Biomaterials 22 : 1531-1539, 2001.
24) Chen RM, Chen TL, Chiu WT, Chang CC : Molecular mechanism of nitric oxideinduced osteoblast apoptosis. J Orthop Res 23 : 462-468, 2005.
25) Henriques LC, de Brito LC, Tavares WL, Vieira LQ, Ribeiro Sobrinho AP : Cytokine analysis in lesions refractory to endodontic treatment. J Endod 37 : 1659-1662, 2011.
26) Kim TG, Lee YH, Lee NH, Bhattarai G, Lee IK, Yun BS, et al : The antioxidant property of pachymic acid improves bone disturbance against AH plusinduced inflammation in MC-3T3 E1 cells. J Endod 39 : 461-466, 2013.
27) Mayahara K, Yamaguchi A, Takenouchi H, Kariya T, Taguchi H, Shimizu N : Osteoblasts stimulate osteoclastogenesis via RANKL expression more strongly than periodontal ligament cells do in response to PGE(2). Arch Oral Biol 57 : 1377-1384, 2012.
28) Tripuwabhrut P, Mustafa M, Gjerde CG, Brudvik P, Mustafa K : Effect of compressive force on human osteoblast-like cells and bone remodelling: an in vitro study. Arch Oral Biol 58 : 826-836, 2013.
29) Barker TH, Baneyx G, Cardó-Vila M, Workman GA, Weaver M, Menon PM, et al : SPARC regulates extracellular matrix organization through its modulation of integrin-linked kinase activity. J Biol Chem 280 : 36483-36493, 2005.
30) Chang PC, Seol YJ, Goldstein SA, Giannobile WV : Determination of the dynamics of healing at the tissue-implant interface by means of microcomputed tomography and functional apparent moduli. Int J Oral Maxillofac Implants 28 : 68-76, 2013.
31) Yamaki K, Kataoka Y, Ohtsuka F, Miyazaki T : Micro-CT evaluation of in vivo osteogenesis at implants processed by wire-type electric discharge machining. Dent Mater J 31 : 427-432, 2012.
32) Karimbux NY, Sirakian A, Weber HP, Nishimura I : A new animal model for molecular biological analysis of the implant-tissue interface: spatial expression of type XII collagen mRNA around a titanium oral implant. J OralImplantol 21 : 107-113, 1995.
33) Buser D, Broggini N, Wieland M, Schenk RK, Denzer AJ, Cochran DL, et al : Enhanced bone apposition to a chemically modified SLA titanium surface. J Dent Res 83 : 529-533, 2004.